A comparison of large eddy simulation models for numerical simulation of airflow in hard disk drives.

Sujit Kirpekar and David Bogy

Computer Mechanics Laboratory

Department of Mechanical Engineering

University of California at Berkeley

Berkeley, CA 94720

kirpekar@newton.berkeley.edu

December 2004.

Table of Contents

Abstract

In modern computer disk drives, tolerances for flow-induced vibrations of the read-write head are getting smaller and smaller. For this reason, significant experimental and computational research is focused on studying the airflow turbulence in such disk drives. Three large eddy simulation models, the Smagorinsky model (Smagorinsky (1963)), the dynamic model (Germano et al (1991)), the localized dynamic model (Menon et al (1997)), and a direct simulation are used to simulate the airflow in hard disk drive enclosures with a single e-block arm as an obstruction. The objective of this work is to compare the performance of these large eddy simulation models and determine which model is best capable of representing the essential physics of the flow. Since very little experimental or direct numerical simulation (DNS) data is available, the scope of this work is limited to comparing LES with a direct simulation on the same grid, which cannot resolve up to the Kolmogorov scale. We provide comparisons in the total kinetic energy, the viscous dissipation at the rotating disks, the energy spectra and some turbulence statistics on the velocity and pressure. It is observed that the total kinetic energies of the simulations asymptote to the same level in spite of differences in the rate of energy input. This indicates that the different mechanisms of production and dissipation of kinetic energy compensate for each other. It is also observed that there is better correlation in turbulence statistics between the direct simulation, the dynamic model and the localized dynamic model, than with the Smagorinsky model. We find the Smagorinsky model is consistently over-diffusive and the direct simulation manifests excessive energy in the small scales. The consequences of this are observable in the deflection of the arm also. Although it is impossible from our data sets to state which, if

any, model generated the “true” behavior, we are able to highlight the important differences between them, which is expected to play a crucial role in the future numerical investigation of airflows in disk drives.

Introduction

The air flow generated due to high speed rotating disks in modern computer disk drives is complicated and contains a range of attributes that require careful attention in a simulation. In today's hard disk drives, there is a trend towards increasing disk rotation speeds and data track density. Current magnetic storage drives operate with speeds of rotation ranging from 7,200 rpm to 15,000 rpm. Unfortunately, the difficulties associated with positioning of read-write heads get compounded with increasing disk rotation speeds. In particular, flow induced vibration of flexible structures get amplified, leading to lesser accuracy in positioning the read-write head (which is flying on a hydrodynamic bearing). For this reason, there has recently been increased interest in both experimental and numerical investigation of the fluid dynamics of disk drives (Shimizu et al (2003), Tsuda et al (2003)).

Large eddy simulation (LES) is an important technique for simulatinge turbulent flows. In LES the large scale motions of the flow are calculated, while the effect of the smaller universal scales (the so called sub-grid scales) are modeled using a sub-grid scale model. LES requires less computational effort than a direct numerical simulation (DNS) but more than Reynolds Averaged Navier Stokes (RANS) methods. Recent studies by the authors (Kirpekar et al (2004)) using the dynamic model to characterize the turbulence field in a disk drive have shown good agreement between experiment and simulation. This paper presents an in-depth comparison of LES models, with an emphasis on accurate simulation of airflows in disk drives.

For disk rotation speeds of 10,000 rpm, the linear velocity U of the outer radius of a 3.5 inch disk is 46.54 m/s. Such high speeds generate high shear stresses at the disks,

causing large amounts of viscous dissipation. If the disk–to-disk spacing h is 3 mm, the Reynolds number based on the disk spacing, at standard atmospheric conditions (density ρ = 1.1614 kg/m^3, dynamic viscosity μ = 1.864e-05 kg/m s), calculated by,

$$\mathrm{Re} = \frac{\rho U h}{\mu} \tag{1}$$

is 8700. The shroud surrounding the rotating disks is also a cause of shear. As has been identified by others (Humphrey et al (1992)) the boundary layer regions immediately adjacent to the rotating disks and shroud are the regions where viscous dissipation is maximum. Typically the read-write heads in disk drives are attached to arms that form an obstruction to the flow. The flow field upstream of the arm (after one complete turn around), has a turbulence intensity of nearly 5-10%. Any change in the upstream turbulence will lead to changes in the pressure fluctuations at the e-block arm, corresponding to a different structural excitation. For this reason, it is important to model the turbulence dissipation (by subgrid transfer and by viscous action) correctly, i.e. the numerical differencing method and sub-grid scale turbulence model should be relatively free of artificial dissipation.

The flow field is also characterized by separation and vortex shedding at the trailing edges of blunt bodies in the flow. This random unsteady shedding of vortices leads to random changes in circulation around these bodies, resulting in unsteady aerodynamic forces. The turbulence model should be able to capture the vortex shedding and the associated form drag.

In modern computer simulations of disk drive enclosures very little attention is paid to the turbulence model used. This is often because, from a user's perspective, the inclusion of a turbulence model in a fluid dynamics calculation can be done very easily in

commercially available CFD codes. On the other hand, there is very little experience in the use of LES models for disk drive airflow simulations. Usually the LES model is chosen indiscriminately, often resulting in less than accurate results. To build credibility into a set of results, it is customary to perform either *a-priori* or *a-posteriori* tests. In the former, experimental or DNS data can be filtered to observe the performance of the LES model and direct comparisons of the predicted SGS stresses can be made. In *a-posteriori* testing, statistics of computed LES solutions may be compared with those obtained by experiments or DNS. Unfortunately for flows in disk drives, limited experimental data Gross (2003) and no DNS data is currently available in the literature, which considerably limits the scope of this exploration. Therefore we are limited to comparing the performance of different LES models only, but this comparison leads to valuable insights about the behavior of these models. We are able to compare the flow fields using these different LES models and relate the properties of the field to the property of the model. Similar comparisons of LES models appear in other works, such as Vreman et al (1997) and Fureby et al (1997). Although these works deal with simple flows there is excellent qualitative agreement in the results. The authors believe this report presents the first such comparison applied to the complicated flows in disk drives. In this paper, we assume the reader is moderately familiar with the LES technique; for an introduction to the practice of LES, we refer the reader to Ferziger (1983), Ferziger (1996) and Roggalo et al (1984).

Mathematical Formulation

Turbulent flows consist of a wide range of length and time scales. The larger scales are more energetic than the smaller scales, and they are responsible for the

transport of conserved quantities. The smaller scales are universal, self similar and are unaware of the mean flow because such information is lost through the energy cascade procedure (Pope (2000)). Hence large eddy simulation uses a filtering approach to resolve only the larger scales of motion and uses a *sub-grid scale* (SGS) model to model the unresolved scales. For an incompressible flow, the filtered Navier Stokes equations are,

$$\frac{\partial\left(\rho\overline{u_i}\right)}{\partial x_i} = 0 \tag{2}$$

$$\frac{\partial\left(\rho\overline{u_i}\right)}{\partial t} + \frac{\partial\left(\rho\overline{u_i u_j}\right)}{\partial x_j} = -\frac{\partial\overline{p}}{\partial x_i} + \frac{\partial}{\partial x_j}\left[\mu\left(\frac{\partial\left(\rho\overline{u_i}\right)}{\partial x_j} + \frac{\partial\left(\rho\overline{u_j}\right)}{\partial x_i}\right)\right] \tag{3}$$

where the over bar indicates the filtering operation[1]. The quantity $\overline{u_i u_j} \neq \overline{u_i}\,\overline{u_j}$ on the left side of Eqn. 3 is unknown and is replaced by $\overline{u_i}\,\overline{u_j}$. The difference between the terms is modeled by an approximation.

$$\tau_{ij} = \left(\overline{u_i u_j} - \overline{u_i}\,\overline{u_j}\right) \tag{4}$$

Here τ_{ij} is called *the sub-grid scale (SGS) stress,* and it represents the interaction of the filtered field with the unresolved field. Different LES models seek to provide an approximation to the SGS stress term, either through an algebraic equation, or by the solution of a differential equation.

The Smagorinsky model

The Smagorinsky model is an algebraic SGS model based on the eddy viscosity hypothesis (gradient diffusion hypothesis) of Boussinesq (1877). The SGS stress is

[1] Filtering involves convolving a quantity with a "filtering kernel" to produce the filtered variable.

related to the filtered strain rate through a single constant called the eddy viscosity, just as the shear stress is related to the strain rate linearly in a Newtonian fluid. If the filtered strain rate is defined as,

$$\overline{S}_{ij} = \frac{1}{2}\left(\frac{\partial \overline{u_i}}{\partial x_j} + \frac{\partial \overline{u_j}}{\partial x_i} \right) \tag{5}$$

and the mean strain rate as,

$$\left|\overline{S}\right| = \sqrt{2\overline{S}_{ij}\overline{S}_{ij}} \tag{6}$$

the SGS stress (most often only the anisotropic part of the SGS stress) is given by,

$$\tau_{ij} = -2\nu_T \overline{S}_{ij}\,, \tag{7}$$

where the eddy viscosity ν_T is evaluated in a way similar to Prandtl's mixing length hypothesis,

$$\nu_T = l_m^2 \left|\overline{S}\right| \tag{8}$$

$$l_m = C_s \Delta \tag{9}$$

in which Cs is the Smagorinsky constant. This gives the final expression for the SGS stress as:

$$\tau_{ij} = -2\Delta^2 C_s^2 \left|\overline{S}\right| \overline{S}_{ij}\,. \tag{10}$$

Thus the Smagorinsky model implies that the SGS stress tensor and the filtered strain rate tensor are aligned and can be related through a single constant Cs. We note that no explicit filtering is needed to implement the SGS model. In our code variable values on the grid are taken as filtered values, which implies the application of a box filter with a (variable) width equal to the cell size. Thus, it is not possible for us to determine an exact filter function to compare our results with DNS, as would be the case with any complex

geometrical simulations. We also note that the turbulence production term, which is the inner product of the SGS stress and the filtered strain, is negative definite implying that energy is being transferred from the large scales to the small scales. This is only qualitatively correct, and it does not allow reverse energy cascades or backscatter. By studying the behavior of the model in the inertial range, various authors have made predictions to estimate the constant Cs. Lilly (1967) first predicted a value of 0.17, others have predicted lower values ranging from 0.065 to 0.1. In our simulation we use Cs = 0.1, as predicted by Piomelli et al (1988).

The dynamic model

The dynamic model, originally due to Germano et al (1991), is also an algebraic SGS model. Here, in addition to the subgrid filtering, another filter called the subtest filter is applied to the flow field. Typically, the width of the subtest filter is chosen to be twice the width of the subgrid filter. Our code uses implicit filtering for the subgrid level, and explicit filtering using a top-hat filter (in all three directions) for the subtest level. We denote the subgrid filtering with a tilde and the subtest filtering with an overbar. Then, using the eddy viscosity hypothesis and a Smagorinsky-type model for the subgrid and subtest stresses, we obtain,

$$\tau_{ij} = \widetilde{u_i u_j} - \tilde{u}_i \tilde{u}_j = -2\tilde{\Delta}^2 C \left|\tilde{S}\right| \tilde{S}_{ij} \tag{11}$$

$$T_{ij} = \widetilde{\widetilde{u_i u_j}} - \overline{\tilde{u}_i}\,\overline{\tilde{u}_j} = -2\overline{\tilde{\Delta}}^2 C \left|\overline{\tilde{S}}\right| \overline{\tilde{S}_{ij}}\,, \tag{12}$$

where we denote the subgrid scale stress by τ_{ij} and the subtest level stress by T_{ij}. Here we have replaced the Cs^2 (in Eqn. 10) by C to allow for the variation of sign. It is easy to see that the Leonard stress tensor defined by,

$$L_{ij} = T_{ij} - \overline{\tau_{ij}} = \overline{\tilde{\tilde{u}}_i \tilde{\tilde{u}}_j} - \overline{\tilde{\tilde{u}}_i}\ \overline{\tilde{\tilde{u}}_j} \tag{13}$$

is a known quantity, and it can be used to evaluate the model constant. The Leonard stress tensor may also be written as,

$$L_{ij} = -2C\left[\overline{\tilde{\tilde{\Delta}}^2 \left|\tilde{\tilde{S}}\right| \tilde{\tilde{S}}_{ij}} - \tilde{\Delta}^2 \overline{\left|\tilde{\tilde{S}}\right| \tilde{\tilde{S}}_{ij}}\right]. \tag{14}$$

This equation may be used to evaluate C, but a single constant C is needed from the 5 independent components of the anisotropic part of L. To overcome this, Lilly (1992) minimized the error using a least square technique. This procedure, however, leads to numerical instabilities, hence most implementations average the coefficient in the homogenous direction, as proposed by Piomelli (1993).

There are several advantages of using the dynamic model compared to the Smagorinsky model. Firstly, the model coefficient is neither prescribed nor remains constant, rather it is determined as a part of the solution. Secondly, the Leonard tensor is zero in laminar flow, giving the correct zero SGS stress. Thirdly, the model predicts a cubic behavior of the SGS stress near the wall, which agrees well with experimental results. Also, the model can do away with *ad hoc* modifications to the SGS near the wall, as is commonly done in the Smagorinsky model. Lastly, the model constant C can take negative values, and hence the model can account for energy transfer in both directions.

The localized dynamic model

The localized dynamic model first proposed by Kim et al (1995) is a one-equation SGS model based on a method of first solving a transport equation for the subgrid scale kinetic energy k.

$$k = \frac{1}{2}\left(\overline{u_i^2} - \overline{u_i}^2\right) \tag{15}$$

$$\frac{\partial k}{\partial t} + \overline{u_i}\frac{\partial k}{\partial x_i} = -\tau_{ij}\frac{\partial \overline{u_i}}{\partial x_j} - \varepsilon + \frac{\partial}{\partial x_i}\left(\upsilon_T \frac{\partial k}{\partial x_i}\right) \tag{16}$$

The three terms on the right hand side of Eqn. 16 represent the production, dissipation and transport of SGS kinetic energy. Here, the SGS stress is modeled using the eddy viscosity hypothesis, the eddy viscosity is modeled using the SGS kinetic energy and dissipation is also modeled using the SGS kinetic energy on dimensional grounds. This procedure is similar to that used in the one-equation Reynolds Averaged methods.

$$\tau_{ij} = -2\nu_T \overline{S_{ij}}$$

$$\nu_T = c_\nu k^{1/2} \overline{\Delta}$$

$$\varepsilon = c_\varepsilon \frac{k^{1/2}}{\overline{\Delta}}$$

in which the model constants c_ν and c_ε are evaluated by applying the dynamic modeling method (as described above) to the kinetic energy equation.

This SGS model removes the mathematical inconsistency of the algebraic dynamic model (having to approximate one constant from five equations), and because the model computes the evolution of SGS kinetic energy, it is capable of capturing non-local and history effects of the turbulence. This is the central advantage of the model over other algebraic models.

Test case used for comparison

For this work we used a computational model consisting of 2 disks, rotating at 10,000 rpm, separated from each other by a gap of 3 mm. A top view of the

computational volume is shown in Figure 1. The gap between the disk outer edge and the enclosing wall (shroud) is 1 mm. A single obstruction in the form of an e-block arm was used. The thickness of the arm is 1 mm, and it was placed symmetrically at the midplane between the disks. The horizontal boundary surfaces of the computational volume at the top and bottom (except the rotating disks), were modeled as an inviscid wall (symmetry plane boundary conditions). The structure was fixed at its back face and thus modeled as a cantilever. Each simulation was started from the same initial conditions, which were obtained from a steady state k-epsilon solution of the average flow.

An unstructured grid, with quadrilateral dominant cells (90% quadrilateral elements, 10% triangular elements) was used. The total number of cells was 245,745, the smallest volume was 6.13e-12 m^3 and the largest volume was 5.41e-10 m^3. A representative grid size of 0.408 mm may be calculated by averaging over all the control volumes as,

$$h = \left(\frac{1}{N} \sum_{N} \Delta V \right)^{\frac{1}{3}} \tag{17}$$

It is important to compare our grid size with the Kolmogorov scale and the Taylor micro-scale. The Kolmogorov scale gives an estimate of the length scale at which dissipation takes place. Ideally, direct numerical simulations resolve the Kolmogorov scale and require no artificial SGS-type dissipation. Using the k-ε method we are able to approximate the dissipation, ε, in our computational volume. Dissipation is obviously a function of position, but when averaged over the entire domain, it is found to be approximately 9.78 x 10^4. We note that this value is in good agreement with the

dissipation predicted by the large eddy simulations (see Table 2). The upper bound on dissipation was 5.64 x 10^5.

We used this average estimate of dissipation to approximate the Kolmogorov length scale, and the velocity and time scales,

$$\eta = \left(\frac{\nu^3}{\varepsilon}\right)^{1/4} = 0.0143\,\text{mm} \tag{18}$$

$$u_\eta = (\varepsilon\nu)^{1/4} = 1.126\ \frac{\text{m}}{\text{s}} \tag{19}$$

$$\tau_\eta = \left(\frac{\nu}{\varepsilon}\right)^{1/2} = 1.267\times10^{-5}\ \text{s} \tag{20}$$

This calculation indicates that our grid size is one order larger than what is needed to resolve the Kolmogorov scale. Hence the direct simulation cannot represent all of the dissipating motions, and therefore we should observe a build up of excessive small scales. This prediction is later confirmed.

Another method to estimate a length scale is the Taylor's microscale, λ. Although it does not have a clear physical meaning (Pope (2000)), the Taylor scale may be used as an estimate of intermediate size eddies (at sufficiently high Reynolds numbers). For calculating the Taylor scale, the size of the largest eddies (L) is taken as the separation distance between the disks, i.e. 3 mm. To approximate the velocity scale of the largest eddies, we use 5% of the disk linear velocity, to obtain,

$$\lambda = L\sqrt{10}\left(\text{Re}_L\right)^{-1/2} = 0.455\ \text{mm} \tag{21}$$

This calculation shows that our grid resolution is sufficient to resolve the Taylor scale. There is excellent agreement of the above length, time and velocity scales with the recent work of Kazemi (2005).

Our study uses a commercial finite volume based code (ESI Software) that uses the SIMPLEC method for solving the Navier Stokes equations. At every time step it integrates the pressure and shear stress on the e-block arm to determine the resultant loading. This is used to determine the dynamic response of the e-block arm as the calculation progresses. Thus a coupled fluid-structure problem is solved. No information about the displacements of the arm (typically less than 10 nanometers) is fed back to the flow solver.

We used second order central differencing in our calculations, with the intention of avoiding the well known dissipative errors of upwind-based methods (Mittal et al (1997)). A time step of 2e-05 was chosen, which allows us to resolve a frequency range up to 25 kHz, which is the range of the essential physics. Implicit Euler's method was used for time advancement.

In order to compare the results from different turbulence models we used the same grid in each simulation. Each simulation was integrated for 2400 time steps, which at 10,000 rpm, corresponds to 8 revolutions of the disks. A conjugate gradient method was used to solve the elliptic Poisson equation for pressure (in the SIMPLE procedure) in all the simulations, and the over-relaxation parameters for each dependant variable (which control the speed of convergence) were the same.

Results and Discussion

Kinetic energy

We define the resolved kinetic energy as,

$$E_f = \frac{1}{2}\overline{u_i}\,\overline{u_i} \tag{22}$$

and a conservation equation for this quantity may be easily derived as:

$$\frac{DE_f}{Dt} - \frac{\partial}{\partial x_i}\left[\overline{u_j}\left(2\nu\overline{S_{ij}} - \tau_{ij} - \frac{\overline{p}}{\rho}\delta_{ij}\right)\right] = -2\nu\overline{S_{ij}}\,\overline{S_{ij}} - \tau_{ij}\overline{S_{ij}} + W \tag{23}$$

When integrated over the entire volume, the second term on the left hand side of Eqn. 23 should be zero. Numerically, however, this term is not zero, and its value is a measure of the numerical dissipation of the simulation. The first term on the right of Eqn. 23 is the viscous dissipation (which is always negative by the second law of thermodynamics) and the second term is the loss of kinetic energy to the residual scales (i.e. production of residual kinetic energy k). This term is always negative for the Smagorinsky model, but it can change sign in the other two models. A positive SGS dissipation term implies the backscatter of energy from small scales to large ones. Direct simulations that do not calculate the SGS stress tensor τ_{ij} have zero SGS dissipation. Finally, the last term on the right hand side, W, is a source term for the kinetic energy, which represents the work done by the rotating disks on the fluid volume. This rate of energy input is equal to the power loss at the disks, which we refer to as windage.

Windage

There is no general agreement on the definition of the term “windage”. Some authors (Tsuda et al (2003)) use the term to imply the disk power loss (in watts), while others use it more generally to refer to “the fluctuating aerodynamic force” (Shimizu et al

(2003)) and some others (Hirono et al (2004)) use “windage” to refer to the flow-induced displacements of the arm. We prefer to use windage to refer strictly to the power loss at the rotating disks due to viscous action. This quantity may be calculated (for each disk) using the expression

$$W = 2\pi\omega\int_0^R \tau_{z\phi} r^2 dr \tag{24}$$

where W is the windage, ω is the angular velocity of the disk, $\tau_{z\phi}$ is the component of the shear stress tensor with the associated force that produces a resultant viscous torque, and R is the disk outer radius.

Discussion

Plotted in Figure 2 is the resolved kinetic energy integrated over the entire volume, and Figure 3 shows the windage. A legend for all of the plots in this paper is given in Table 1. We note that there is very little difference in the global kinetic energy between the different turbulence models. This implies that the main features of the resolved flow are reasonably independent of the SGS model. This is in good agreement with Fureby et al (1997). However, the direct simulation predicts approximately 1-5% lesser kinetic energy. On the other hand, as seen in Figure 3, the energy input into the system (i.e. the windage) is about 20% more for the dynamic model and localized dynamic model, and about 15% more for the Smagorinsky model, as compared to the direct simulation. This indicates that there are significant differences in the energy transfer mechanisms of these simulations. Clearly, the direct simulation has the least amount of energy input from the disks (W), but it exhibits kinetic energy comparable to the LES simulations. This is because the direct simulation lacks a mechanism to transfer

energy to the unresolved scales (τ_{ij} is zero) which leads to the accumulation of too many small resolved scales. On the other hand, there is less than 1% difference in the kinetic energy between the dynamic model, the localized dynamic model and the Smagorinsky model, but an approximate 5% difference in their energy input rates. This indicates that although the Smagorinsky model has lesser energy input per unit time, it bears almost the same kinetic energy as the dynamic model. More insight into this discrepancy can be obtained by considering the way each model resolves the wall layer.

For practical considerations the first grid point from the wall in our simulations was maintained at $8 < y^+ < 20$. This ensures that the first grid point is between the viscous sublayer and the inertial sublayer. In our code the Smagorinsky constant is damped near the wall using the well known van Driest damping function (van Driest (1956)).

$$C_s = C_s(1 - e^{y^+/A}), \tag{25}$$

where A is taken to be 26, as customary. The dynamic models do not use any damping functions and are known to display the correct asymptotic behavior at the wall (Germano et al (1991)). This indicates that the Smagorinsky model's wall functions (which have no physical grounds, and are implemented only to agree with experimental results) are inaccurate in representing the velocity field close to the disks (hence the shear stress at the disks, and correspondingly the windage). Thus more confidence may be placed in the results due to the dynamic models, and we conclude that the Smagorinsky model is not accurate in representing the energy flow into the system, and this may have serious consequences on the physics of the flow.

Finally, we observe that the global kinetic energy of all simulations asymptote to the same value, which indicates that our simulations have a tendency to equilibrate to the

same energy level although there exist differences between the amount of energy inputted per unit time. This is a surprising result, and it suggests that different energy production (windage) and dissipation (SGS dissipation, viscous dissipation and numerical dissipation) mechanisms have compensated each other. For this reason, the physics of these flows are reasonably similar in the mean.

Mean and RMS fluctuations of azimuthal velocity and pressure

The azimuthal and radial velocities can be decomposed into their mean and fluctuating components. Turbulence intensity is a non-dimensional quantity representing the ratio of the root mean square (rms) of the fluctuation to the mean flow speed. We calculate the mean and rms components of the azimuthal velocity, starting the averaging at 2 revolutions and ending it at 8 revolutions of the disk, i.e. averaging over 6 revolutions, or 1800 time steps.

We plot these turbulence statistics along four radial chords in the flow domain, each of them located midway between the disks (see Figure 4). The chord 1 lies in the turbulent wake formed behind the arm, and the chords 2, 3 and 4 are at successively increasing angular positions along the direction of rotation of the disk. Mean flows are plotted for each chord in Figure 5-8. RMS values of fluctuations are plotted in Figure 9-12. Finally, the ratio of the two, i.e. turbulence intensity is plotted in Figure 13-16. To generate these figures, we used data at 10 points (12 points for chord 1) along the chord and a shape preserving spline interpolant was fit through the points. For all chords, zero represents the inner boundary at the hub, and one represents the other boundary at the shroud.

We note that the regions close to the disk hub in Figure 16 representing chord 4 should be neglected from this analysis. The *mean* flow speed is small near the hub (often the flow reverses direction) resulting in large turbulence intensity (which is calculated using the mean flow in the denominator). Such turbulence intensity values (of the order of 100%) are unphysical.

For chord 1 we see that there is better agreement in the mean velocities and the rms fluctuations predicted by the direct simulation and the dynamic models, than with those predicted by the Smagorinsky model. We observe that the Smagorinsky model predicts significantly smaller fluctuations, which is an indication of its diffusive nature.

The same observations apply to chords #2, 3 while at chord #4 the difference between the mean velocities predicted by the models becomes insignificant. From all the figures illustrating the rms fluctuations of velocity we can conclude that the Smagorinsky model has a tendency to predict lower fluctuations than the other turbulence models. This is evidence of the well known fact that the Smagorinsky model is overly diffusive and delays the transition of laminar to turbulent flow.

The above analysis is also consistent with our global kinetic energy diagram in Figure 2. The smaller fluctuations of the Smagorinsky model do not affect the total kinetic energy too much – fluctuations which are 5% of the mean contribute only 0.25% to the total kinetic energy.

Finally, plotted in Figure 17-20 are the mean pressures along the chords 1-4 and in Figure 21-24 the rms values of pressure fluctuation are plotted along chords 1-4. Very little variation in the mean pressure is consistently observable. Also, the Smagorinsky model shows smaller fluctuations in the wake (chord 1), and the direct simulation shows

larger fluctuations in the other three locations (chords 2, 3 and 4). This has an effect on the vibrations of the e-block arm, as will be discussed subsequently.

Energy Spectra

The spectrum of kinetic energy is useful in demonstrating the distribution of energy among the various scales of motion. For flows with simple geometries and/or periodic domains, obtaining a kinetic energy spectrum is straightforward. However, in our test case, the turbulence is inhomogeneous, and the mean flow is hard to define. In general, the problem does not lend itself to theoretical analysis. To obtain a turbulence spectrum we measure the azimuthal velocity at a particular point in the domain as a function of time. Using Taylor's frozen field hypothesis[2], we convert this time history to a spatial history, and use this data to obtain a (one dimensional, scalar) spatial auto-correlation function,

$$R(x) = \langle u_\theta(x_0) u_\theta(x_0 + x) \rangle \tag{26}$$

where the brackets indicate averaging over all x_0. The Fourier transform of this function represents the one dimensional kinetic energy spectrum as a function of wavenumber (k). To the authors' knowledge, this is the first instance where a turbulence spectrum of the airflow in a disk drive has been studied, and it provides valuable confirmation of the existence of an inertial cascade.

According to Kolmogorov's law of universal equilibrium the energy spectrum E(k) should scale as,

[2] Taylor's hypothesis is based on the assumption that the time scale of turbulent evolution is much slower than the time scale of the mean flow. This is valid if the fluctuations are comparably smaller than the mean flow. We can then assume that the turbulent field is "frozen" and is simply advected by the mean flow. In this analysis, we ensure that the standard deviation of the velocity is not more than 10% of the mean. The error in the kinetic energy spectrum associated with such an approximation is not easy to quantify.

$$E(k) = C\varepsilon^{\frac{2}{3}} k^{-\frac{5}{3}} \tag{27}$$

where C is a constant of order unity, ε is the dissipation rate (rate of energy transfer through the cascade process) and k is the wavenumber. In our case the dissipation ε (which traditionally has units of [length^2/time^3]) may be taken to be the windage per unit mass. It is hypothesized to be independent of wavenumber k, hence we use the average value of windage for estimating ε. These values of ε are in good agreement with our preliminary k-ε calculation. The values of ε calculated by different SGS models are listed in table 2.

Figure 25 shows the kinetic energy spectra obtained using the different models. These have been constructed by using velocity data at a single point in the wake of the arm. Spectra based velocity data at other points in the drive do not show significant differences from those in Figure 25. Firstly, all spectra show rough agreement with the -5/3rd law (see thick line in Figure 25) demonstrating the existence of an inertial sub-range. We observe that the Smagorinsky model curve drops off faster than those of the dynamic model and the localized dynamic model indicating the dissipation of energy at higher wavenumbers. Also, the energy spectrum corresponding to the direct simulation contains the most energy at high wavenumbers, indicating that there is an excessive build up of small scales due to the lack of an SGS model.

Theoretically, a more logical comparison can be made between LES and DNS energy spectra. If the filter function is known in wavenumber space an LES spectrum may be divided by the square of this function, to obtain the equivalent “unfiltered” spectrum. In our simulations, however, the top-hat filter is anisotropic and

inhomogeneous in all three directions. The use of a one dimensional function to represent such a filter is not accurate and hence we refrain from making such a comparison.

There is also very little difference in the spectra predicted by the localized dynamic model and the dynamic model. The localized dynamic model has the advantage of computing a transport equation for SGS-k, which should include non-local and history effects. However, on a sufficiently fine grid such as ours the assumption of equality between production and dissipation appears to be valid, and very little difference is observed in the flow fields of the dynamic model and the localized dynamic model. Finally, we observe that there is significant variation in the model coefficients both in space and time, for the dynamic model (C) and the localized dynamic model (c_ν and c_ε). The Smagorinsky model is unable to capture this local variation. However, this spatial and temporal variation cannot be interpreted easily; hence we refrain from plotting it.

Vibrations

Often the off-track vibrations of the e-block arm or the slider are the most desired results of such a coupled fluid-structure simulation. Hence we compare the vibrations predicted by the simulations. The off track vibrations of the tip of the e-block arm are plotted in Figure 26 as a function of time. The mean and peak-to-peak amplitudes of vibrations are given in Table 3. The mean is calculated by averaging over the final 6 revolutions of the disk, and the peak-to-peak is defined as the difference between the maximum and minimum deflection during this period. We observe that the Smagorinsky model, which predicts a slightly higher mean displacement also predicts the least peak to peak oscillations. Clearly, this is a direct result of the reduced pressure fluctuations. On the other hand, the direct simulation, due to its excessive fluctuations, records a smaller

mean displacement and larger peak-to-peak oscillations. Although the difference in vibration values predicted by the simulations are small (less than 1 nm), we note that these trends will get amplified several times when more realistic structures such as suspensions and sliders are included in the simulation and the sliders off-track vibrations are compared.

Figure 27 shows the frequency spectra of the off-track vibrations shown in Figure 26. In all 4 cases we see the same modes (which correspond to sway and torsion) are excited in the structure. (Peaks are observed at 6.6 kHz, 7.5 kHz, 10 kHz, 1.12 kHz and 1.195 kHz.)

Comparison of computational cost

Large eddy simulations of disk drive airflows need to be computed until the turbulence field achieves a statistically steady state and sufficient time has elapsed for the important modes of the structure to be excited. This typically requires that the computations be carried out for 6-10 revolutions of the drive. Additionally the dynamics of interest lies in the 0-25 kHz range, which limits the size of the time step. As a result, such calculations take a substantial length of time on desktop workstations, ranging from a couple of weeks to more than a month. In this context, the cost of each turbulence model becomes important. In Table 4 we compare the normalized cost per time step of each turbulence model with a Navier Stokes solution on the same grid. This data has been obtained on a desktop Pentium 4 computer running at 3.2 GHz with 2 GB of RAM. The dynamic model is 33% more expensive than the Smagorinsky model and the localized dynamic model is 25% more expensive than the dynamic model.

Conclusions

The study of large eddy simulation SGS models is of considerable interest to the future research in airflow simulations in disk drives. We have presented an investigation of three SGS models, under the limitations of a commercial CFD code. These models occur almost invariably in popular CFD software and their inclusion in a calculation is very easy. We provide *a posteriori* tests of the Smagorinsky model, the dynamic model and the localized dynamic model. By examining various turbulence statistics and measures like the kinetic energy and the energy spectrum, we are able to draw useful conclusions about the performance of each model.

We conclude that the Smagorinsky model does not correlate well with the direct simulations in terms of mean and fluctuating velocities and pressures. We see a better correlation between the dynamic model, the localized dynamic model and the direct simulation. We also observe that there is very little difference between the results predicted by the dynamic model and the localized dynamic model. The Smagorinsky model has a tendency to predict the highest dissipation at small scales, and this leads to smaller fluctuations in velocity and pressure. This extra dissipation leads to smaller peak-to-peak oscillations of the e-block arm, and we anticipate that the errors in vibration results of the structure would be amplified by the addition of slender and more flexible structures like the suspension and the slider. The direct simulation does not resolve up to the Kolmogorov scale, and hence it lacks a mechanism to dissipate energy, which would have ideally taken place at the Kolmogorov scale. This leads to excessive energy at small scales and results in larger fluctuations. Due to this unphysical feature the structure displays more peak to peak oscillations.

The best choice for turbulence modeling appears to be either the dynamic model or the localized dynamic model since they agree well with the direct simulation in the mean and do not show the over dissipation of the Smagorinsky model at the small scales. However, the localized dynamic model requires the computation of SGS-k, which makes it the most expensive choice. This cost is not justified when compared to the results of the dynamic model, and hence we advocate the use of the dynamic model in future. As mentioned earlier, we cannot say which model delivers the “true” physical behavior, but our effort to compare the models has revealed significant differences between them. Future disk drive simulations will need to deal with systems that have high speeds and small scale physics and turbulence models shall play a crucial role in them.

Acknowledgements

This work was supported by the Computer Mechanics Laboratory at the University of California at Berkeley.

References

Ferziger J. 1983. Higher Level simulations of turbulent flows. In *Computational methods for turbulent, transonic and viscous flows*: Cambridge University Press

Ferziger J. 1996. In *Simulation and modeling of turbulent flows.*, ed. TB Gatski, YM Hussaini, JN Lumley: Cambridge University Press

Fureby C, Tabor G, Weller HG, Gosman AD. 1997. A comparative study of subgrid scale models in homogenous isotropic turbulence. *Physics of Fluids* 9: 1416-1429

Germano M, Piomelli U, Moin P, Cabot W. 1991. A dynamic sub-grid scale eddy viscosity model. *Physics of Fluids A*: 1760-1765

Gross H. 2003. *Off-Track Vibrations of the Read-Write Heads in Hard Disk Drives*. University of California, Berkeley

Hirono Y, Arisaka T, Nishijima N, Shimizu T, Nakamura S, Masuda H. 2004. Flow induced vibration reduction in HDD by using a spoiler. *IEEE Transactions on Magnetics* 40: 3168-3170

Humphrey JAC, Shuler CA, Iglesias I. 1992. Analysis of viscous dissipation in disk storage systems and similar flow configurations. *Physics of Fluids A* 4: 1415-1427

Kazemi M. 2005. *Numerical modeling of magnetic head positioning error due to flow-suspension interactions in disk drives.* University of Virginia, Charlottesville

Kim W, Menon S. 1995. *A new dynamic one-equation subgrid-scale model for large eddy simulations*. Presented at 33rd Aerospace sciences meeting and exhibit, Reno, NV

Kirpekar S, Bogy D. 2004. Characterization of turbulence in hard disk drives using large eddy simulation.

Lilly DK. 1967. *The representation of small-scale turbulence in numerical simulation experiments*. Presented at Proceedings of IBM Scientific Computing Symposium on Environmental Sciences, Yorktown Heights

Lilly DK. 1992. A proposed method of the Germano sugrid scale closure method. *Physics of Fluids A*: 633-635

Menon S, Kim W. 1997. Application of the Localized Dynamic Subgrid Scale Model to Turbulent Wall-Bounded Flows. *AIAA Paper* 97-0210

Mittal R, Moin P. 1997. Suitability of upwind-biased finite difference schemes for large-eddy simulation of turbulent flows. *AIAA Journal* 38: 1415-1417

Piomelli U. 1993. High Reynolds number calculations using the dynamics subgrid scale stress model. *Physics of Fluids* A6: 1484-1490

Piomelli U, Moin P, Ferziger JH. 1988. Model consistency in the large eddy simulation of turbulent channel flows. *Physics of Fluids* 31: 1884-1891

Pope S. 2000. *Turbulent Flows*: Cambridge University Press

Roggalo RS, Moin P. 1984. Numerical simulation of turbulent flows. *Annual Review of Fluid Mechanics* 16: 99-137

Shimizu H, Shimizu T, Tokuyama M, Masuda H, Nakamura S. 2003. Numerical simulation of positioning error caused by airflow induced vibration of head gimbals assembly in hard disk drive. *IEEE Transactions on Magnetics* 39: 806-811

Smagorinsky J. 1963. General circulation experiments with the primitive equations, 1. The basic experiment. *Monthly Weather Review* 91

Tsuda N, Kubotera H, Tatewaki M, Noda S, Hashiguchi M, Maruyama T. 2003. Unsteady analysis and experimental verification of aerodynamic vibration mechanism of HDD arms. *IEEE Transactions on Magnetics* 39: 819-825

van Driest ER. 1956. On turbulent flow near a wall. *Journal of Aerospace Science* 23: 1007

Vreman B, Geurts B, Kuerten H. 1997. Large-eddy simulation of the turbulent mixing layer. *Journal of Fluid Mechanics* 339: 357-390

Tables

SGS Model	Line Type in figures
Smagorinsky model	Full line
Dynamic model	Dashed line
Localized dynamic model	Dotted line
Direct simulation	Dash-dotted line

Table 1: Legend for figures

SGS Model	ε
Smagorinsky model	101212.701
Dynamic model	104219.471
Localized dynamic model	104448.123
Direct simulation	88461.554

Table 2: Average dissipation predicted by different SGS models

SGS Model	Mean (nm)	Peak-to-Peak (nm)
Smagorinsky model	3.3838	1.2138
Dynamic model	3.1425	1.4965
Localized dynamic model	3.2445	1.5947
Direct simulation	2.9156	1.7805

Table 3: Mean and peak-to-peak vibrations of e-block arm tip as predicted by different SGS models

Method	**Normalized cost per time step**
Direct simulation (same grid)	1
Smagorinsky model	1.253
Dynamic model	1.677
Localized dynamic model	2.1

Table 4: Normalized cost of different SGS models per time step

Figures

List of Figures

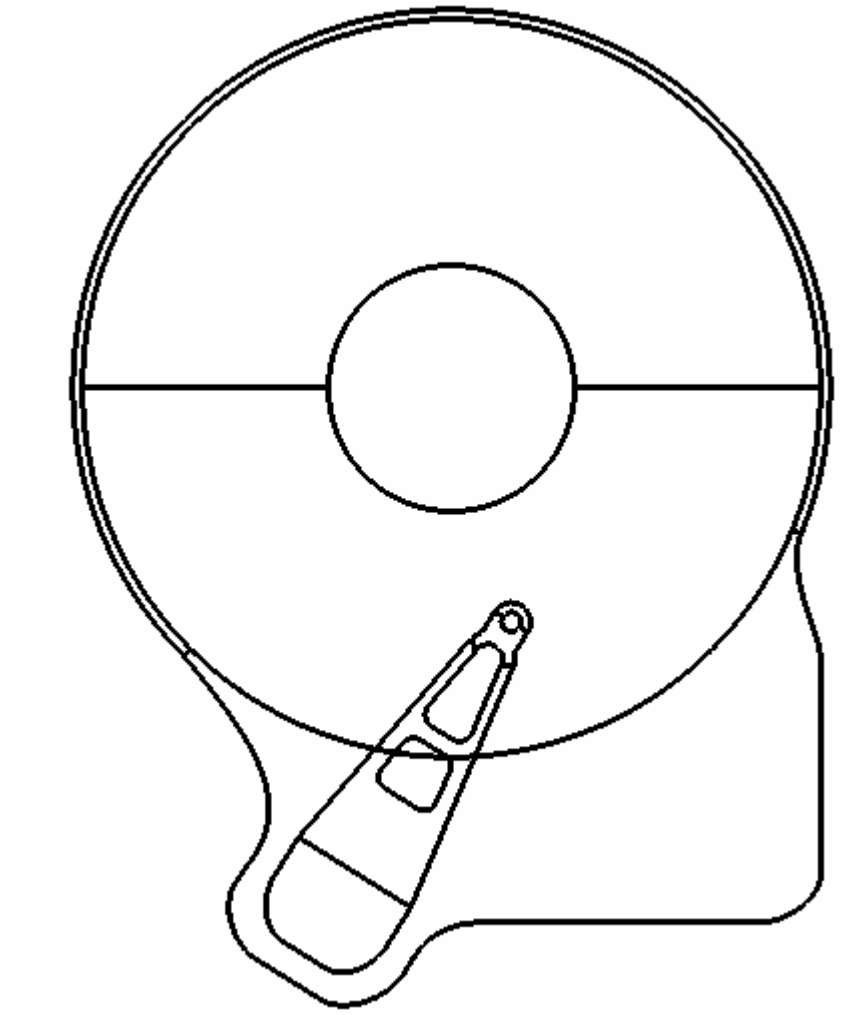

Figure 1. Top view of compuational model

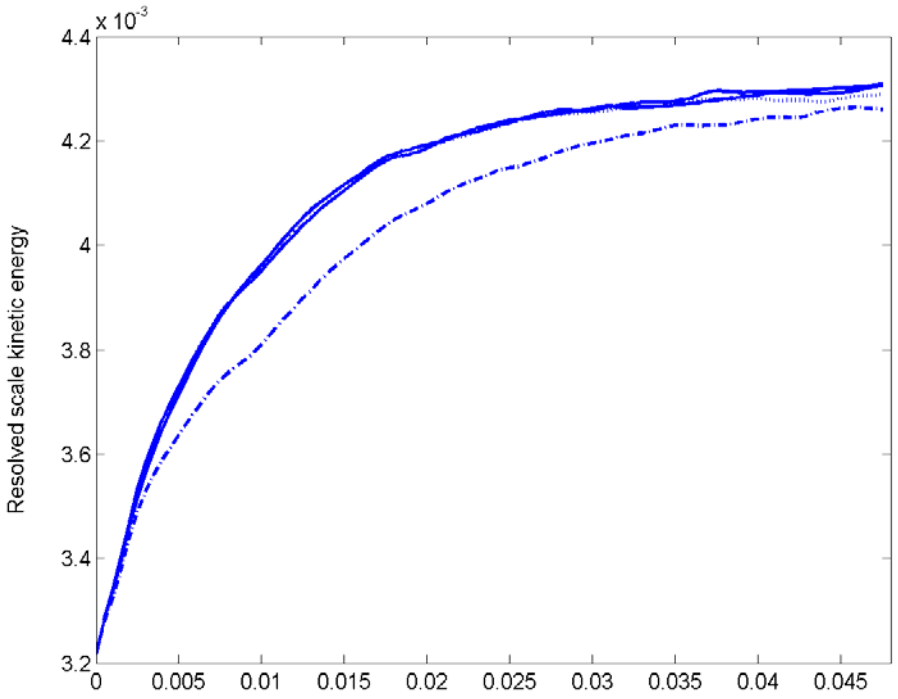

Figure 2. Resolved scale kinetic energy (see table 1 for legend)

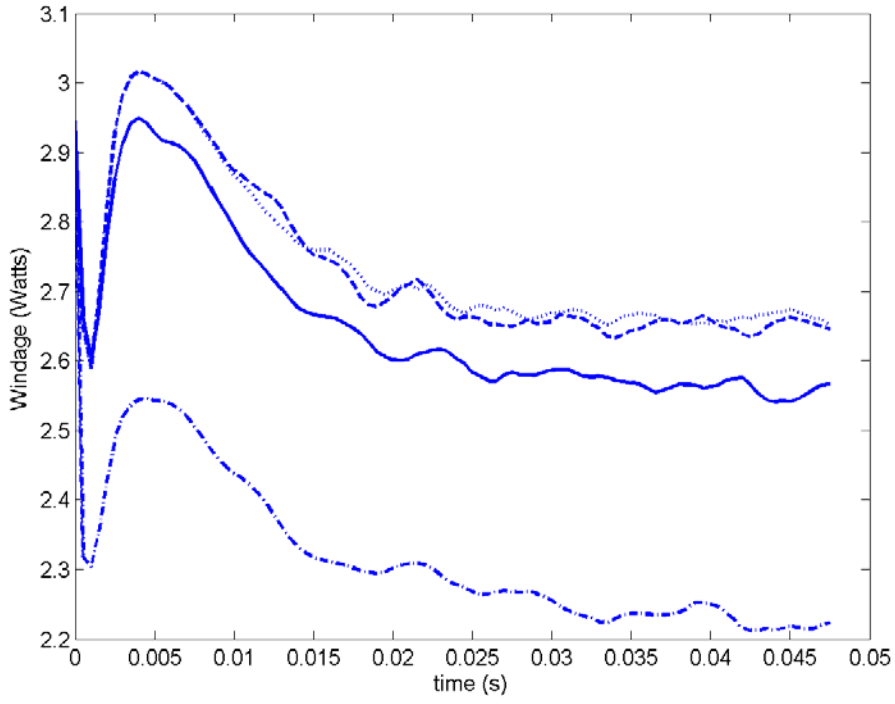

Figure 3. Windage (Watts) (see table 1 for legend)

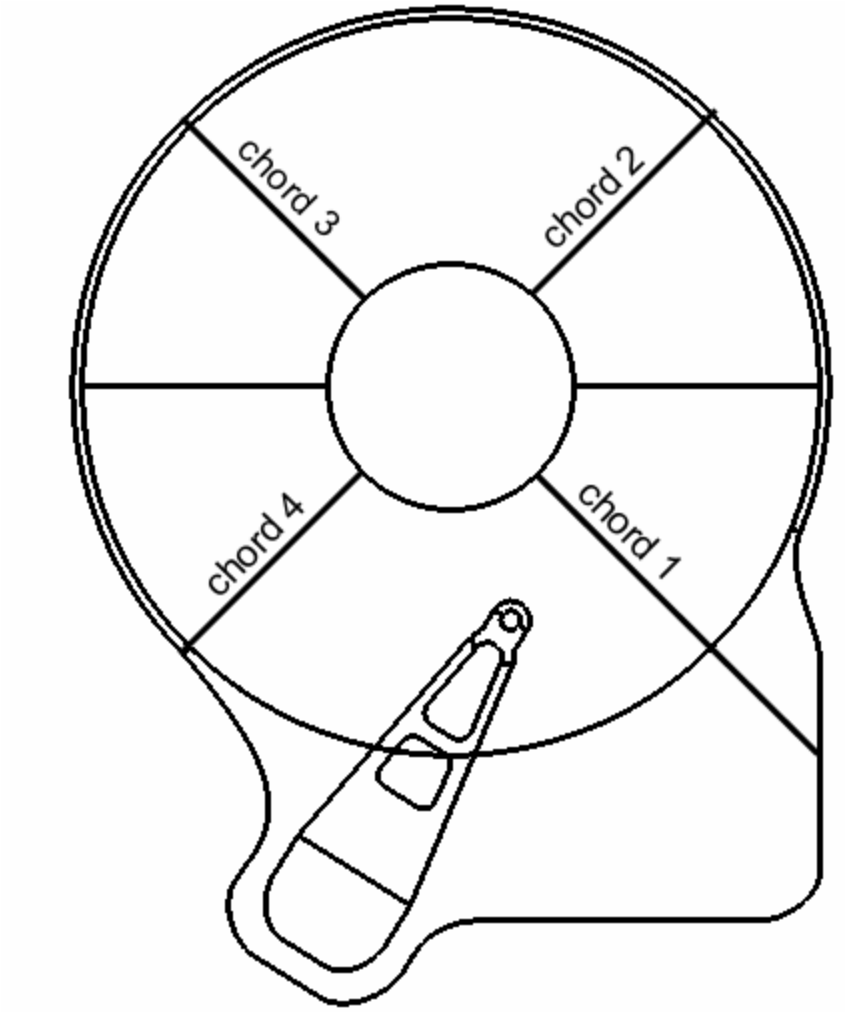

Figure 4. Location of radial lines (chords) for plotting turbulence intensity

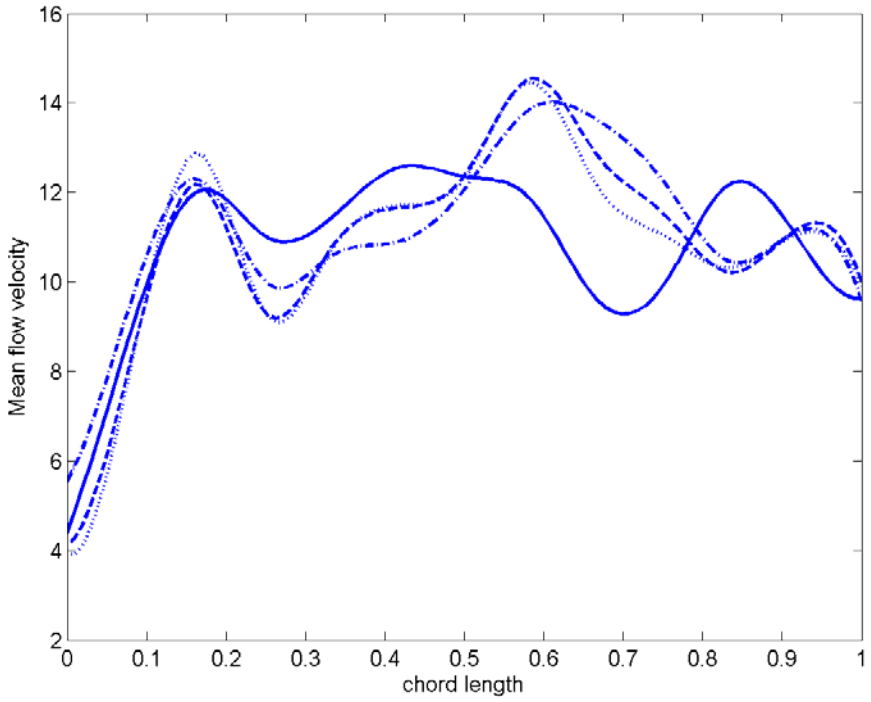

Figure 5. Mean azimuthal flow velocity along chord 1 (m/s) (see table 1 for legend)

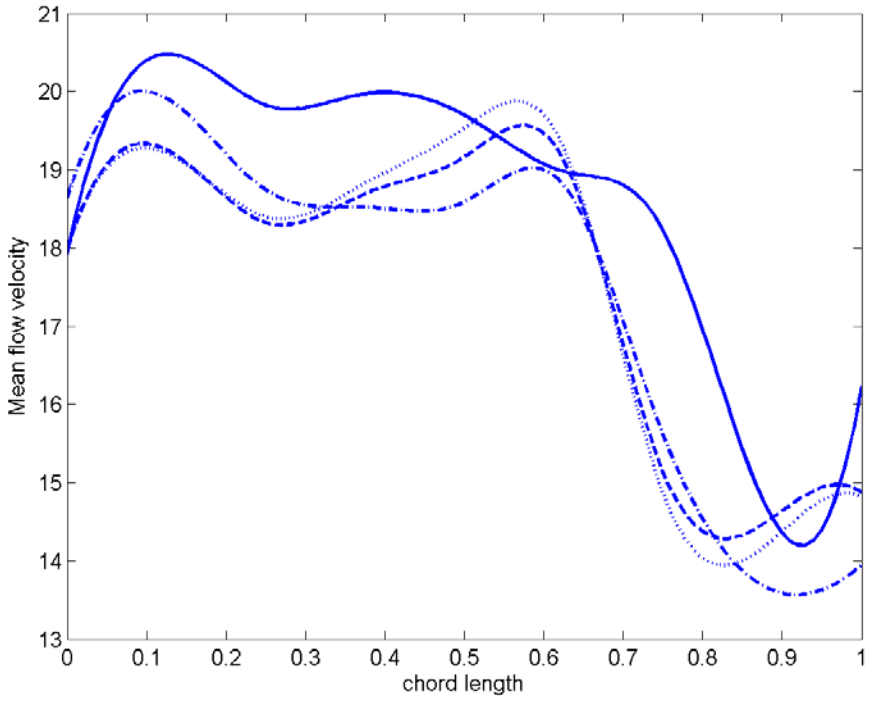

Figure 6. Mean azimuthal flow velocity along chord 2 (m/s) (see table 1 for legend)

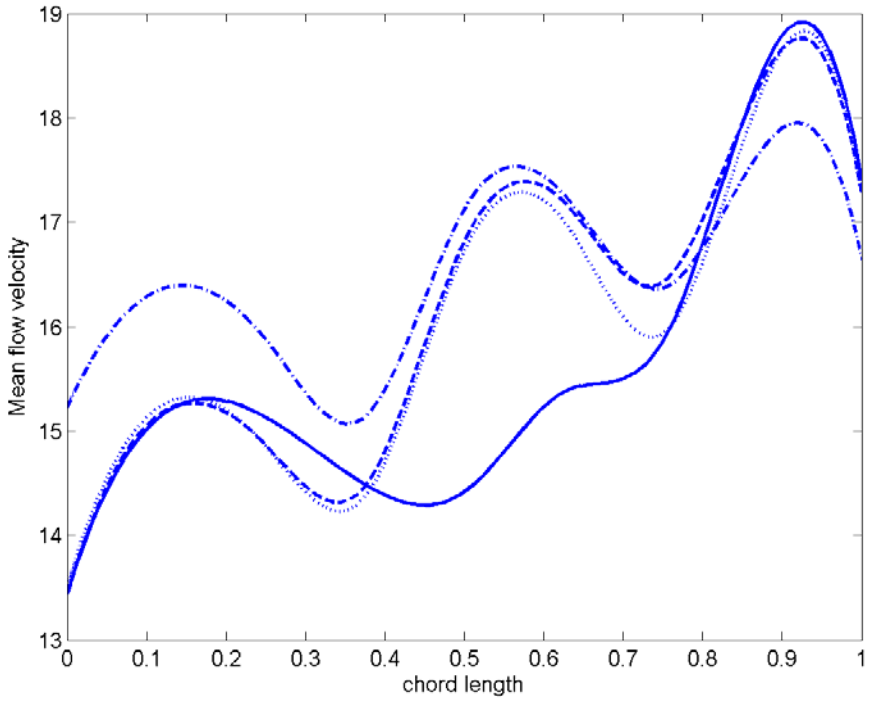

Figure 7. Mean azimuthal flow velocity along chord 3 (m/s) (see table 1 for legend)

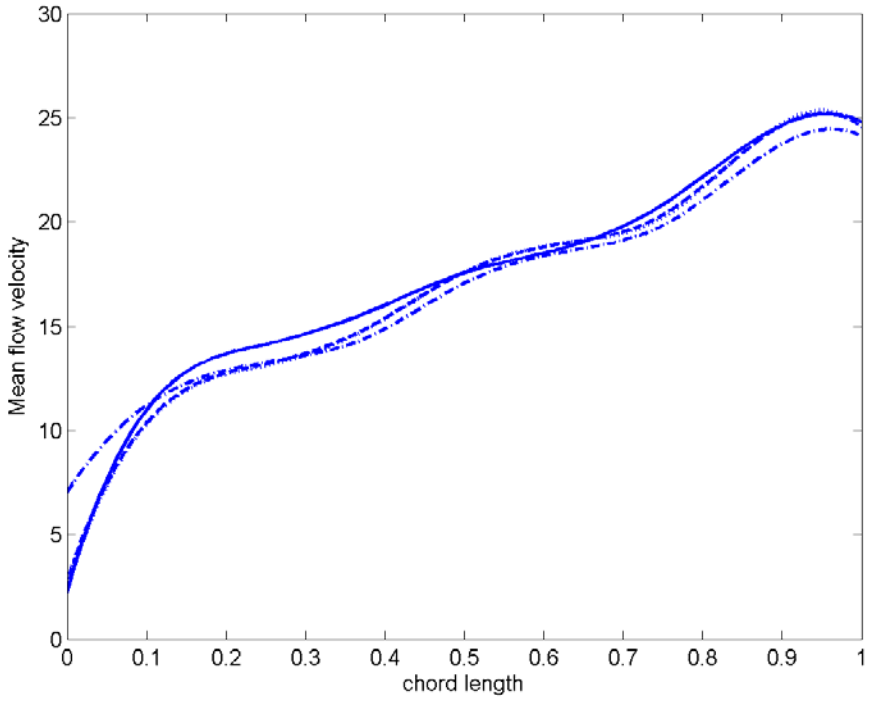

Figure 8. Mean azimuthal flow velocity along chord 4 (m/s) (see table 1 for legend)

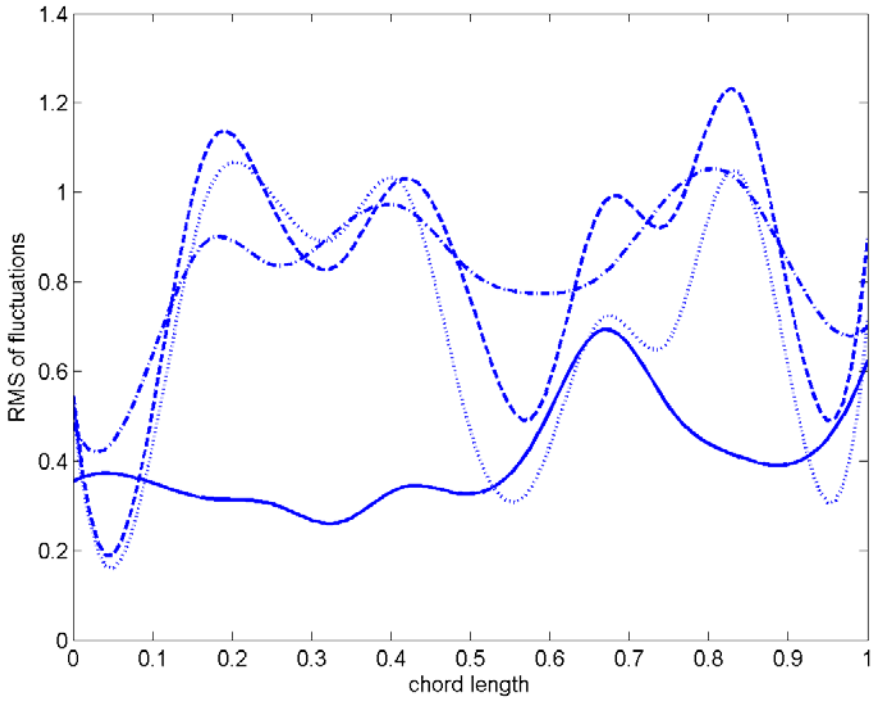

Figure 9. RMS fluctuating azimuthal velocity along chord 1 (m/s) (see table 1 for legend)

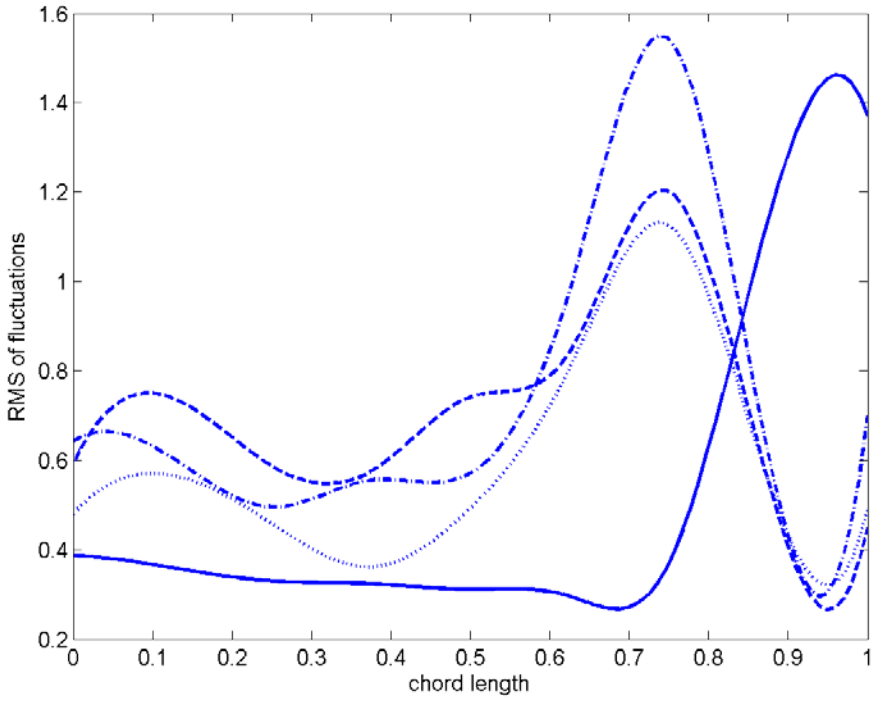

Figure 10. RMS fluctuating azimuthal velocity along chord 2 (m/s) (see table 1 for legend)

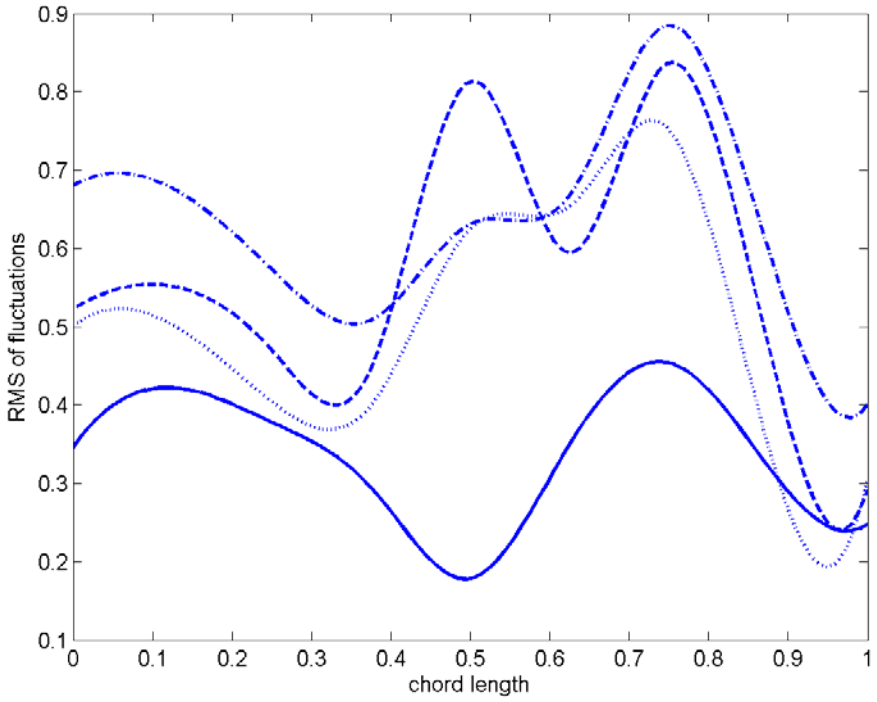

Figure 11. RMS fluctuating azimuthal velocity along chord 3 (m/s) (see table 1 for legend)

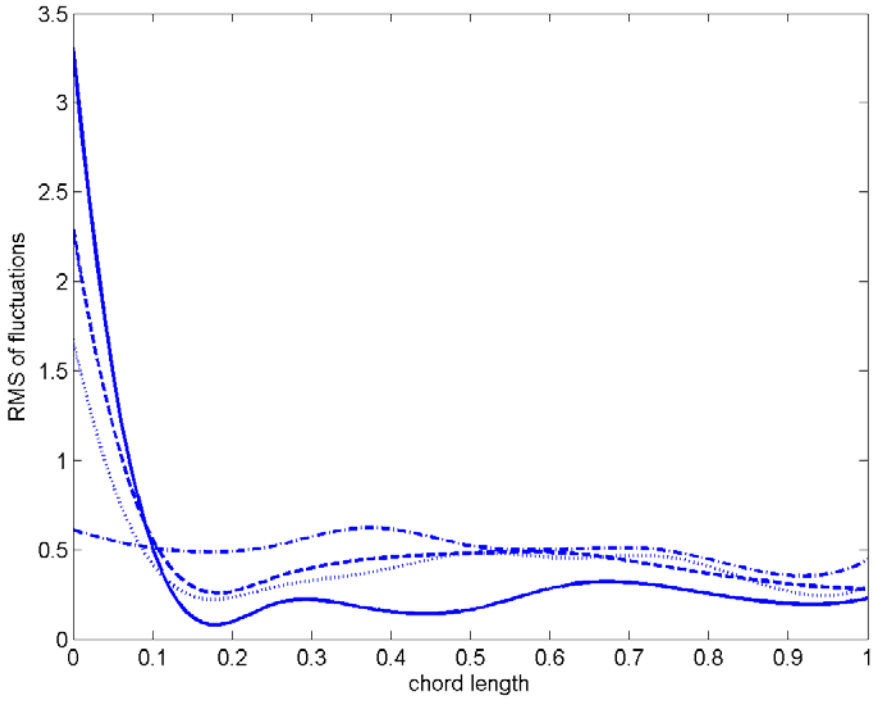

Figure 12. RMS fluctuating azimuthal velocity along chord 4 (m/s) (see table 1 for legend)

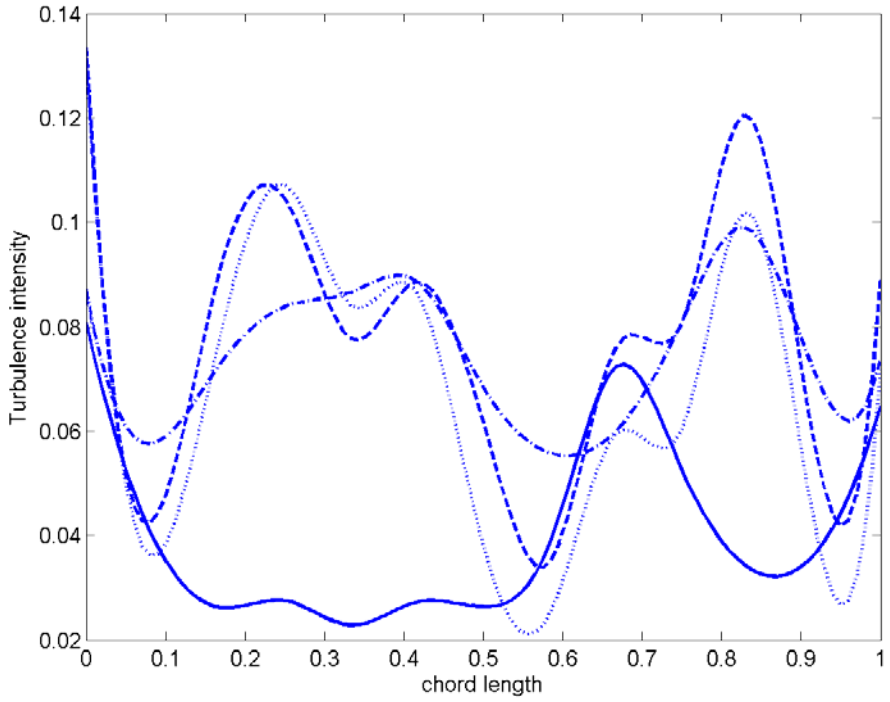

Figure 13. Turbulence Intensity along chord 1 (see table 1 for legend)

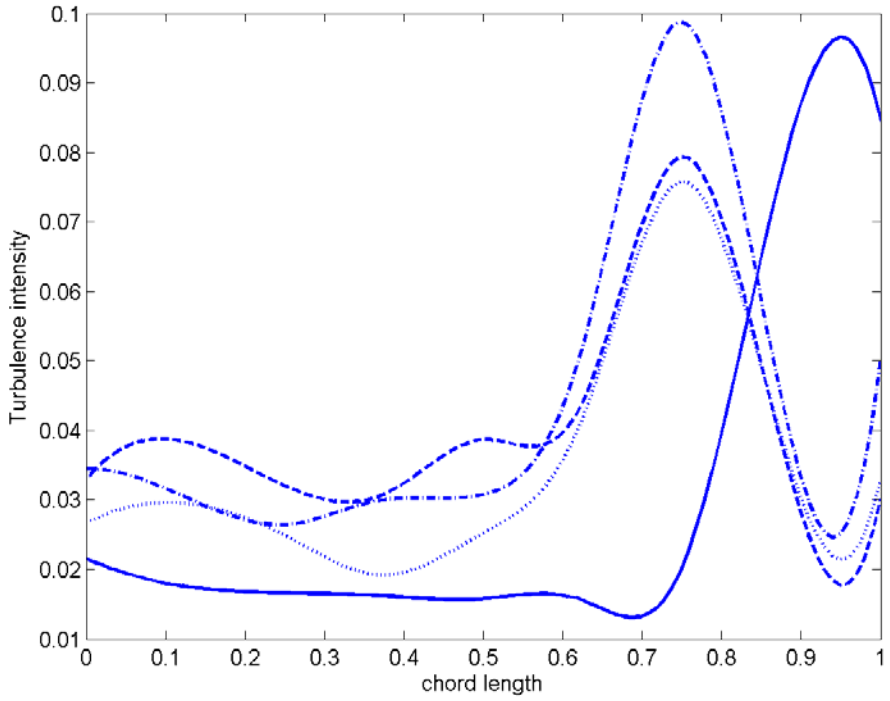

Figure 14. Turbulence Intensity along chord 2 (see table 1 for legend)

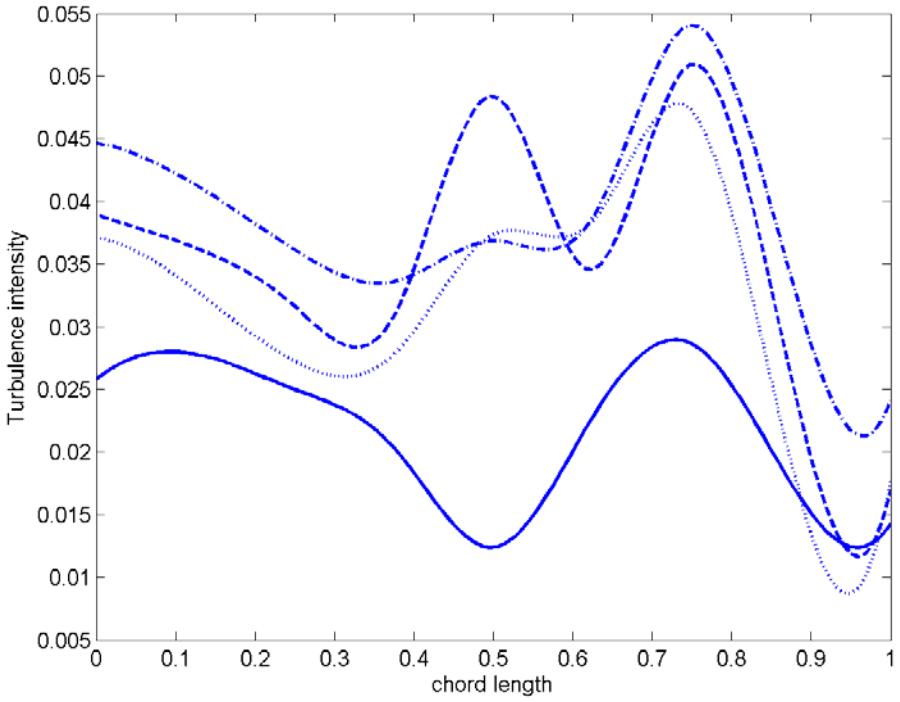

Figure 15. Turbulence Intensity along chord 3 (see table 1 for legend)

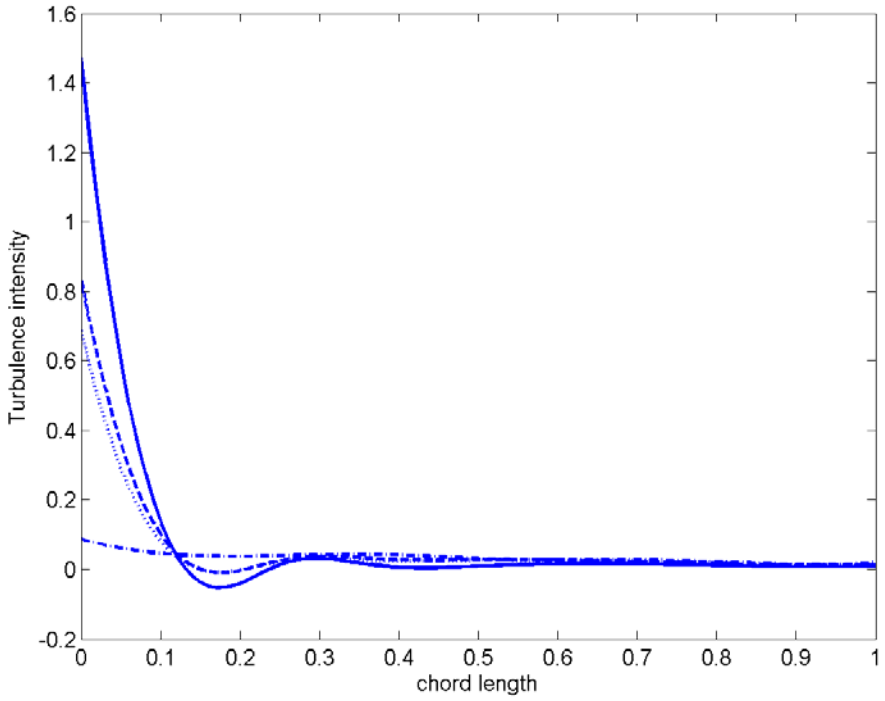

Figure 16. Turbulence Intensity along chord 4 (see table 1 for legend)

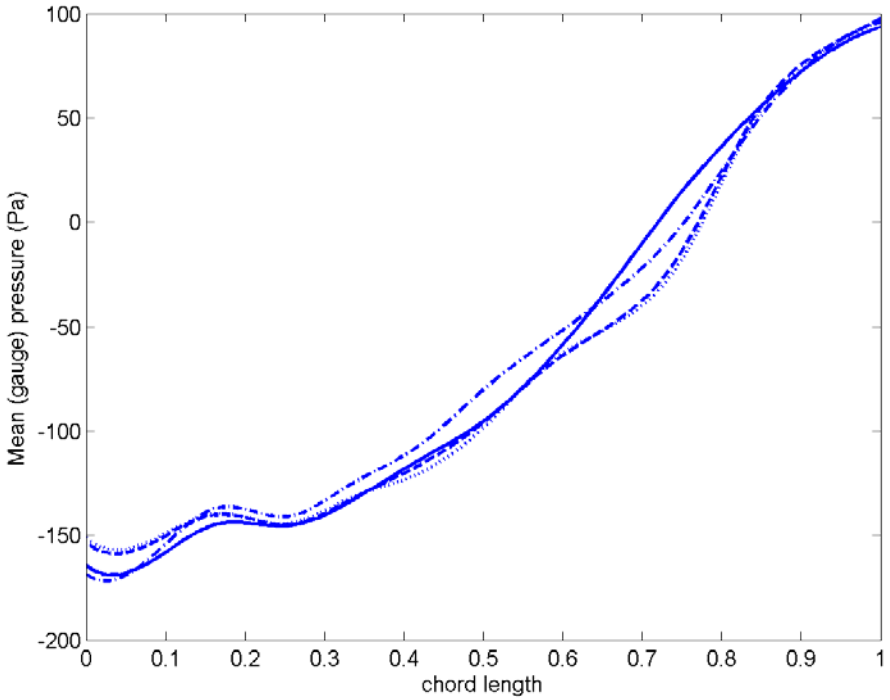

Figure 17. Mean pressure along chord 1 (Pa) (see table 1 for legend)

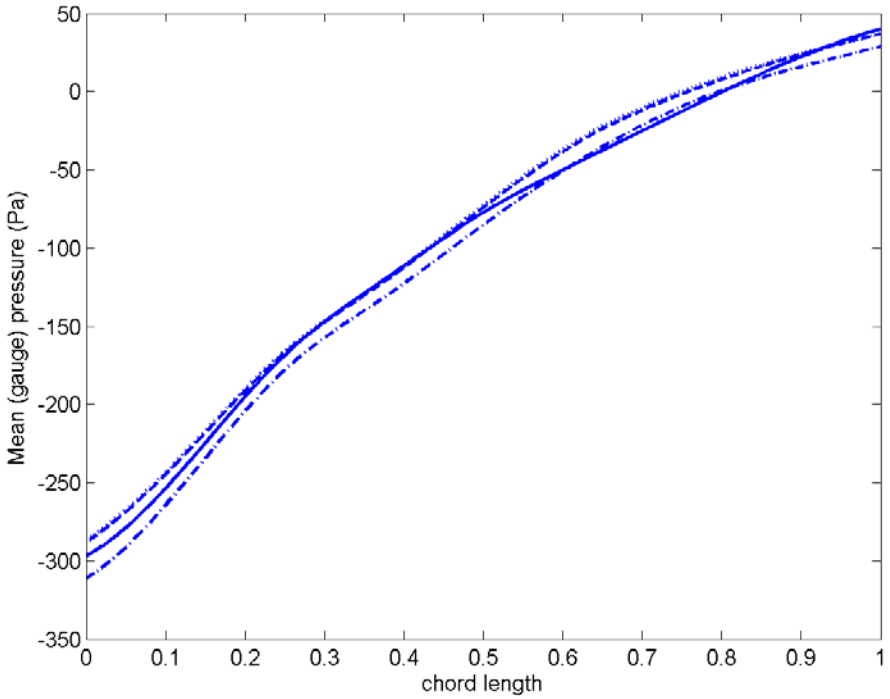

Figure 18. Mean pressure along chord 2 (Pa) (see table 1 for legend)

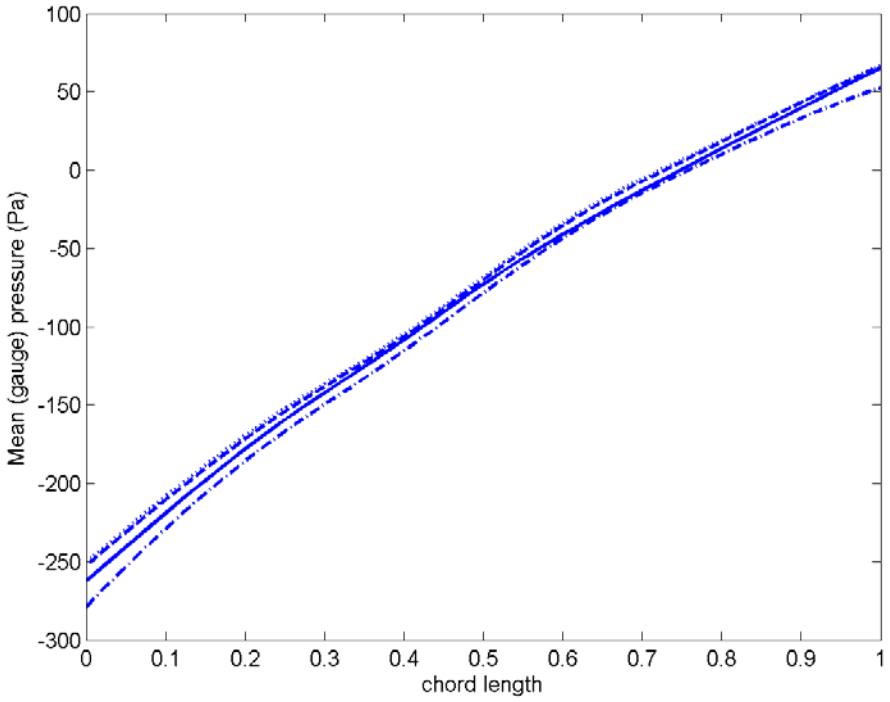

Figure 19. Mean pressure along chord 3 (Pa) (see table 1 for legend)

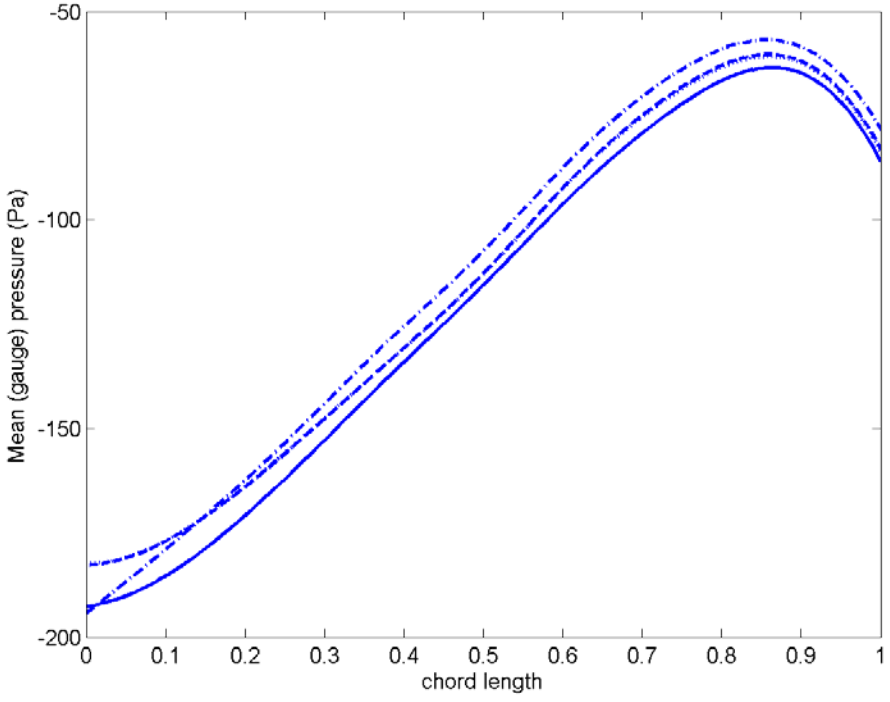

Figure 20. Mean pressure along chord 4 (Pa) (see table 1 for legend)

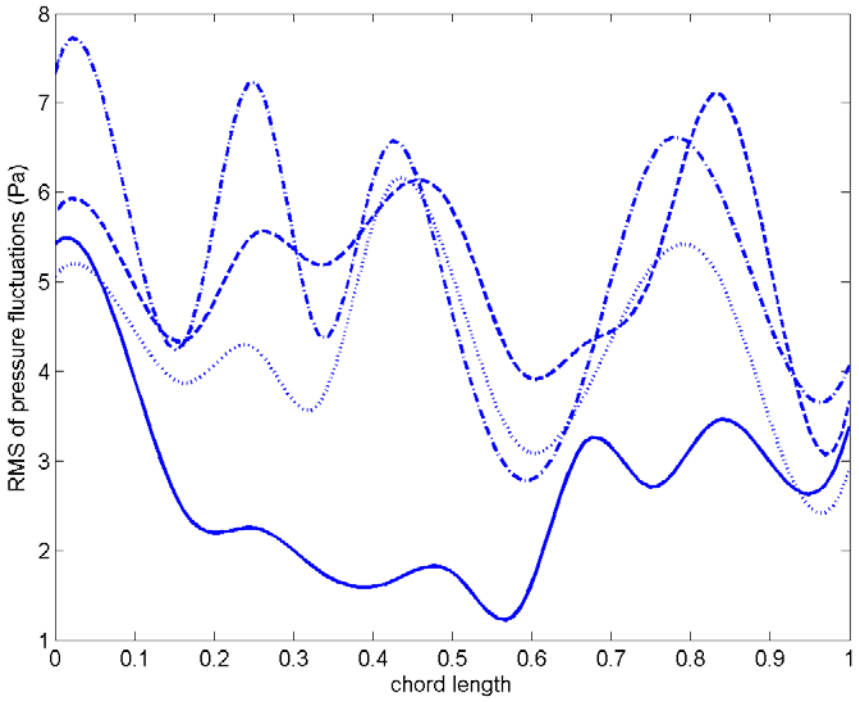

Figure 21. RMS of pressure fluctuation along chord 1 (Pa) (see table 1 for legend)

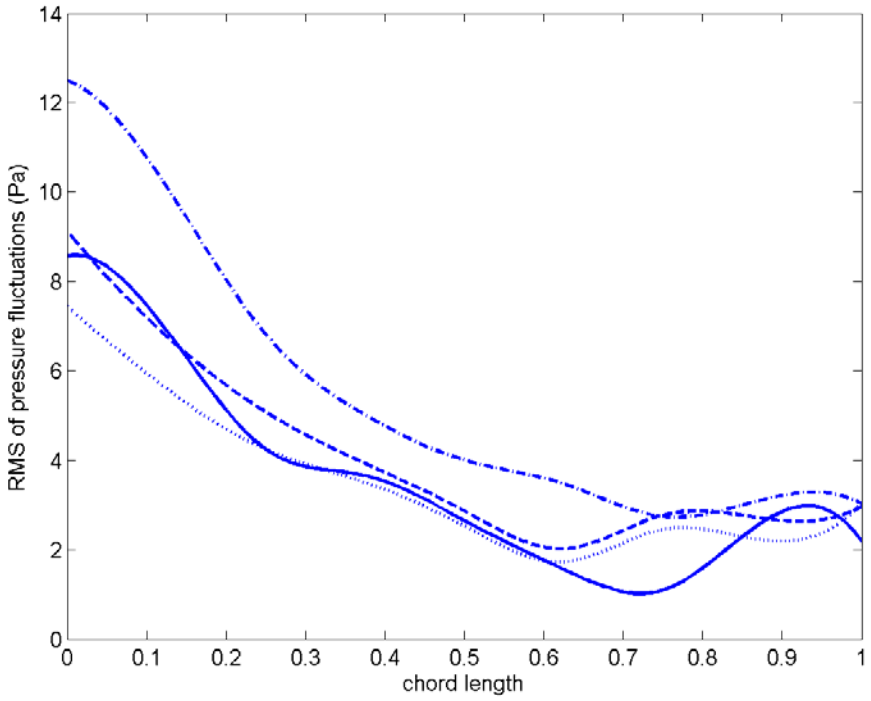

Figure 22. RMS of pressure fluctuation along chord 2 (Pa) (see table 1 for legend)

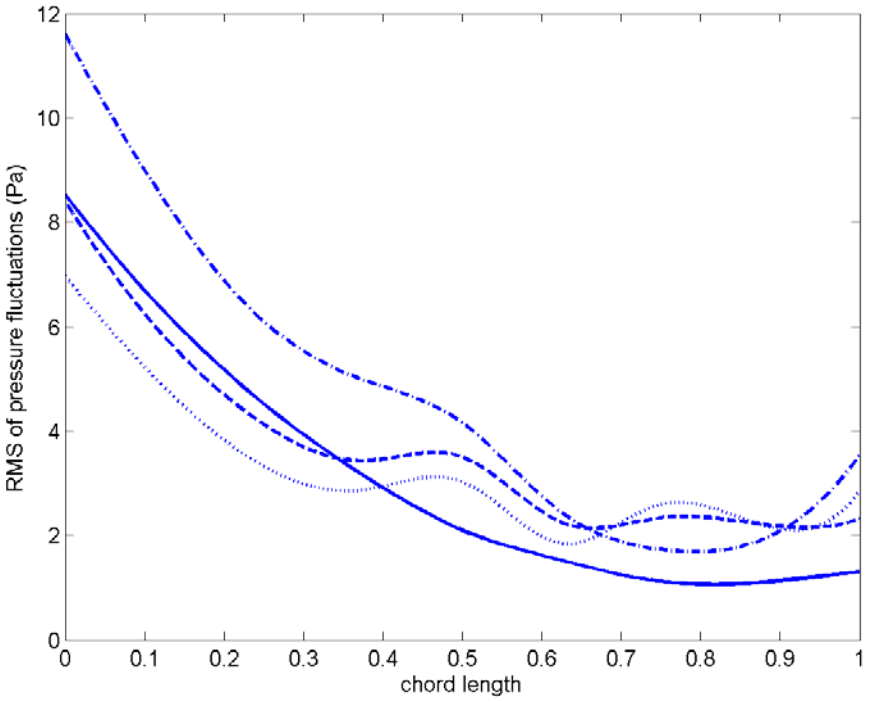

Figure 23. RMS of pressure fluctuation along chord 3 (Pa) (see table 1 for legend)

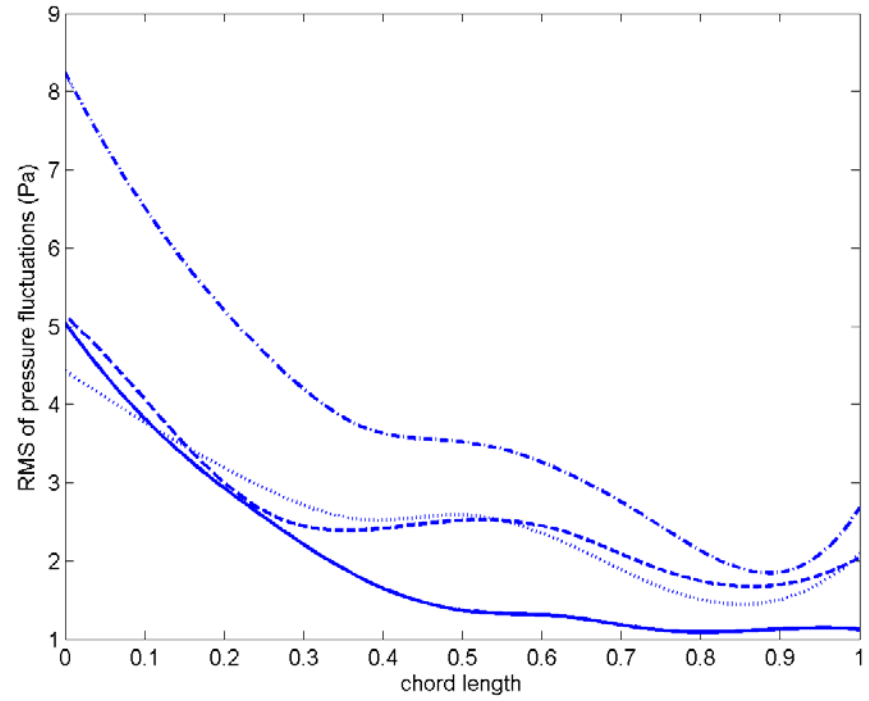

Figure 24. RMS of pressure fluctuation along chord 4 (Pa) (see table 1 for legend)

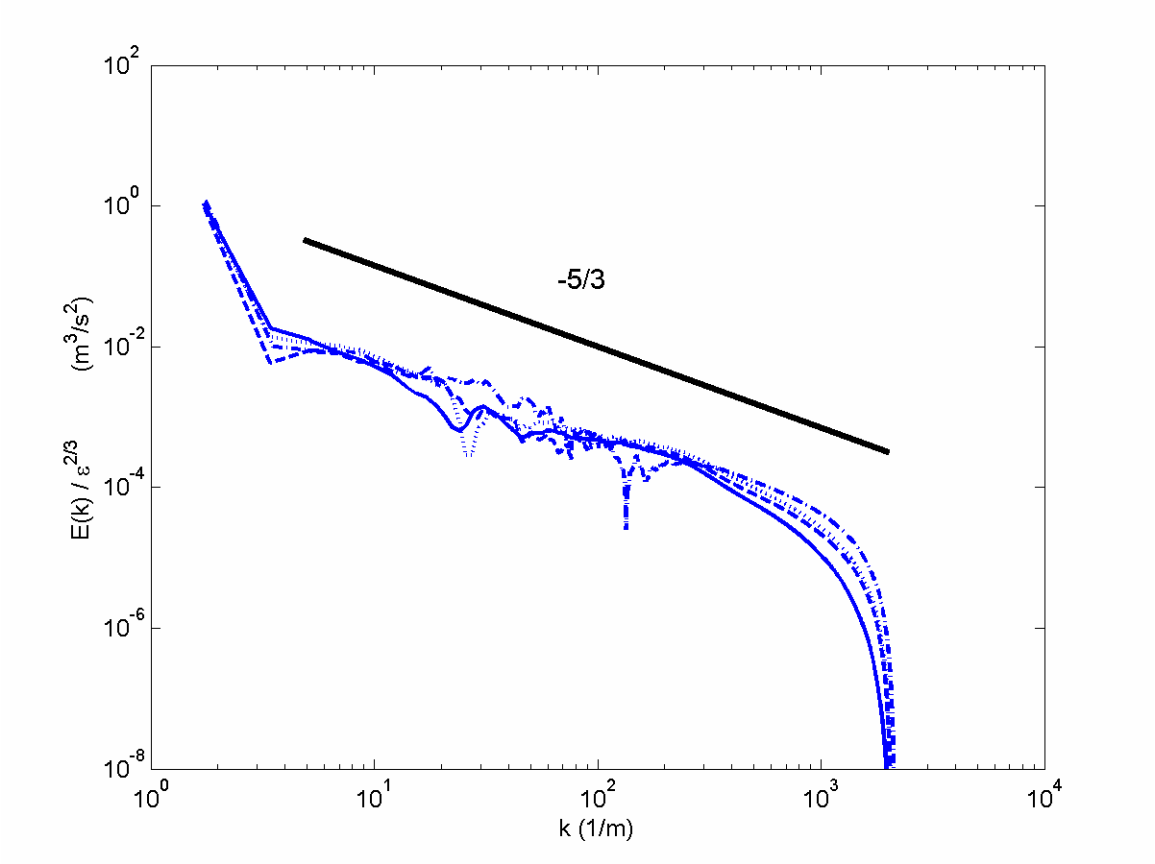

Figure 25. Kinetic energy spectra (see table 1 for legend)

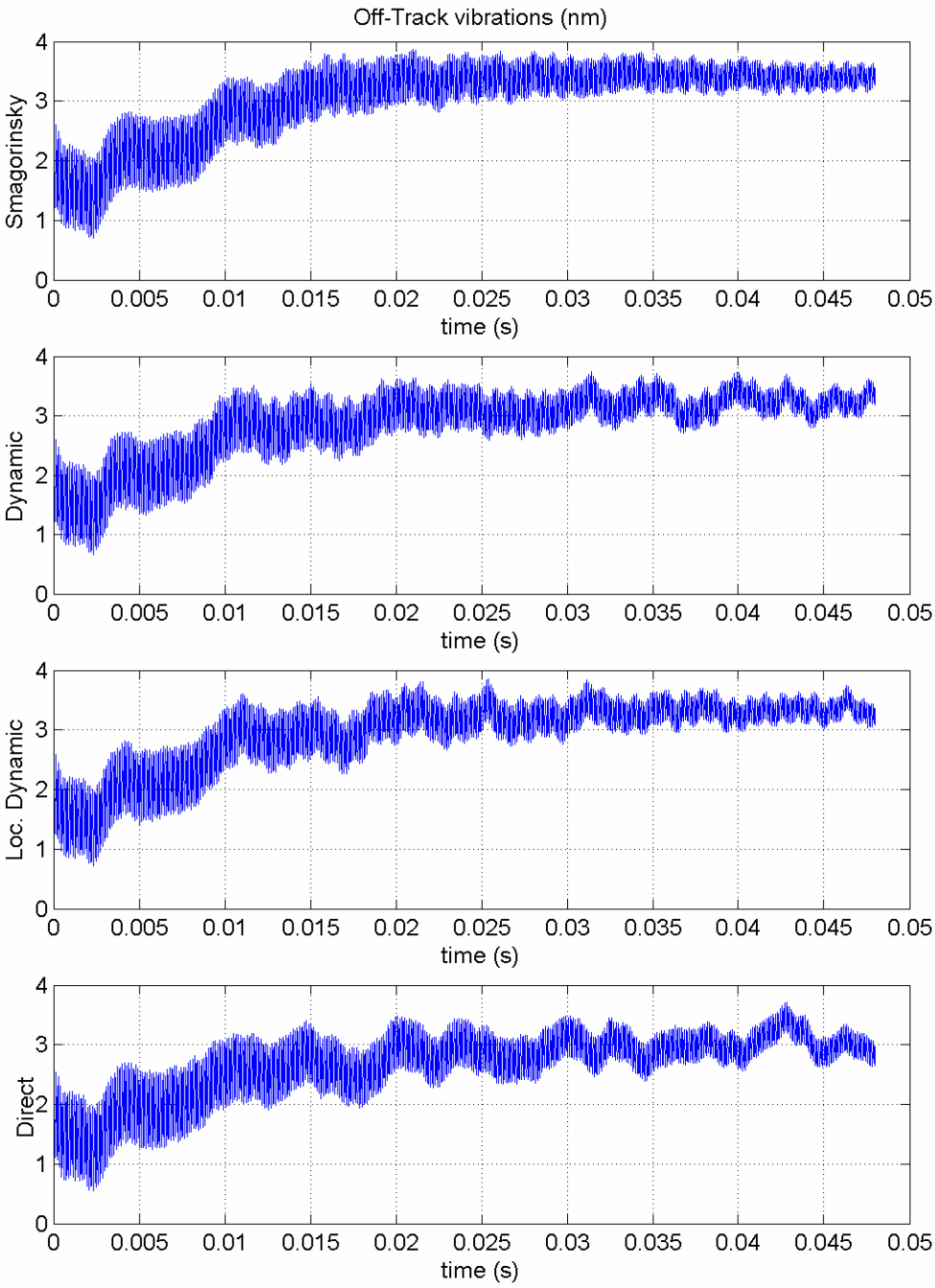

Figure 26. Off-Track vibrations of e-block arm tip

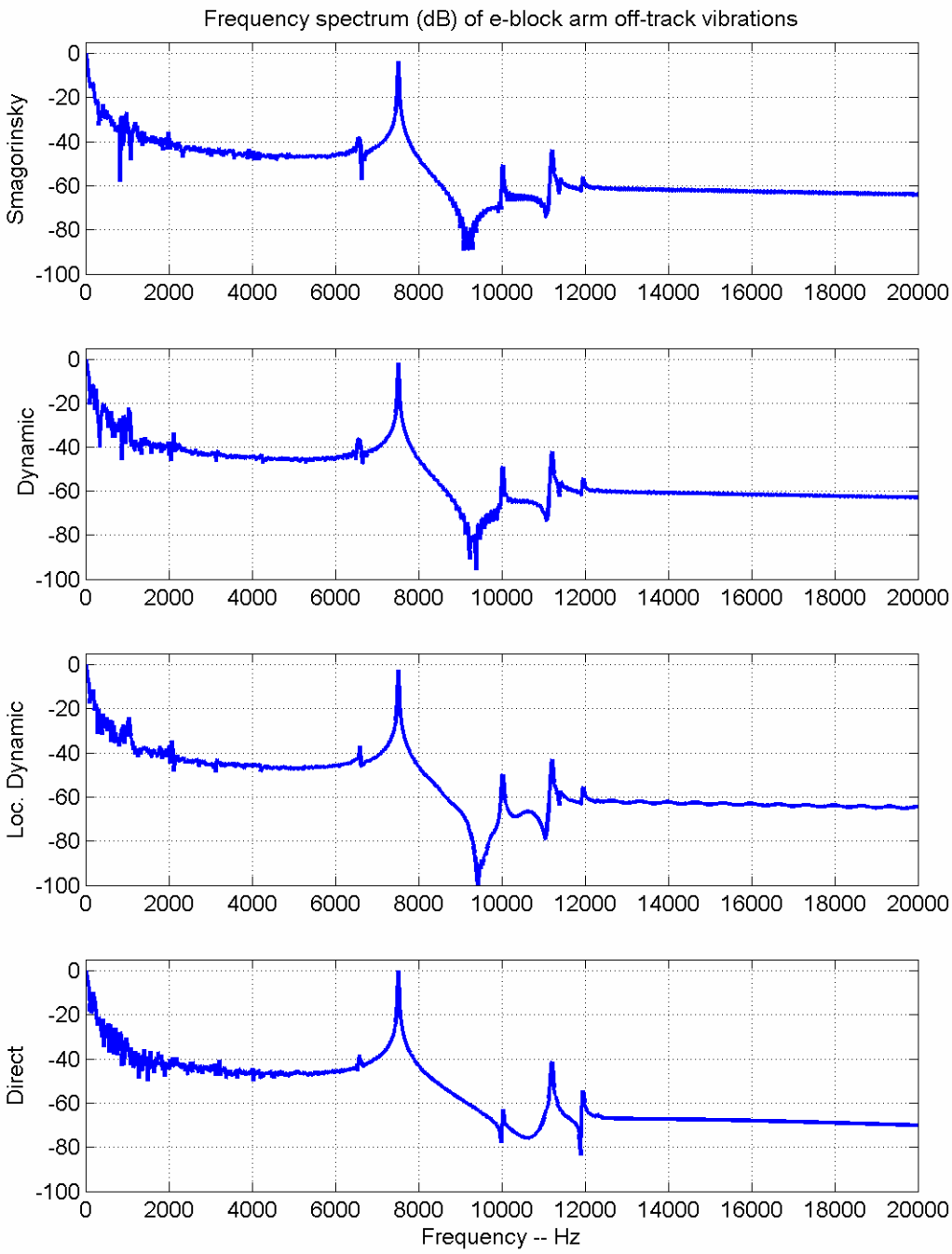

Figure 27. Frequency spectra of e-block arm off-track vibration